High temperature oxidation of iron aluminide coatings

Daniel D.M.R. Ferreira[a], Frederico A.P. Fernandes[b]

Abstract

The corrosion phenomenon on a metal is defined as a destructive and non-intentional attack, normally occurring at the surface. Pack aluminizing is a thermochemical surface treatment often applied to improve the corrosion resistance of alloys. It relies on gaseous and solid state diffusion to form aluminide layers on the substrate. The purpose of the present work is to apply the pack aluminizing treatment to the AISI 304L steel, characterize the produced layers and study its high temperature oxidation resistance. Stainless steel samples were pack aluminized in different conditions at a fixed temperature. The specimens were then submitted to quasi-isothermal oxidation at 1173 K in an opened furnace. Scanning electron microscopy and X-ray diffraction were applied to characterize both oxidized and as-aluminized samples. The pack aluminized layers were mainly composed by the FeAl and/or $FeNiAl_5$ depending on the processing conditions. High temperature response depends on the aluminizing treatment parameters and the oxidation kinetics of the layers containing the FeAl iron aluminide is considerably slower than the observed for the base steel.

Keywords: Pack aluminizing, Iron aluminides, High temperature corrosion.

Introduction

Oxidation is a type of corrosion phenomenon [1] which happens especially on characteristic atmospheres with high concentration of oxidizing compounds. Considering the reaction products that passes through the combustion chamber and then reaches the turbine stage, on a Turbofan engine, it is known that those gases can reach up to 1623 K [2], a suitable environment to form an oxide film on a metal therefore lowering engine's performance. Another problem involving this phenomenon occurs on rocket thrusters. The formation of an oxide layer on a metal changes its internal geometry therefore harming its performance as well [3].

Pack aluminizing is one of the possible solutions for this problem and its implications in high temperature oxidation are studied in the present research. The process applies a powder mixture containing the metal to be diffused into the substrate, an activator, which transports the metal to the sample surface, not being consumed during the process, and an inert compound. The theoretical approach used is based on the *Levine* and *Caves* model [4,5], which is grounded on gaseous and solid diffusion.

Oxidation kinetics are divided in two different mechanisms. The logarithmic kinetics mechanism used is from H. Uhligh works [6] and the parabolic kinetics mechanism, from Wagner's theory of oxidation [7]. The purpose of this research is to identify if pack

[a] Undergraduate, Aerospace Engineering - UFABC
[b] PhD, Materials Engineering - UFABC

aluminizing provides good solutions for high temperature oxidation, and what pack configuration is more effective.

Methodology

The applied alloy was an AISI 304L austenitic stainless steel with the following composition: Fe (18,060 wt%), Cr (8,040 wt%), Mn (1,800 wt%), P (0,037 wt%), Si (0,300 wt%), S (0,024 wt%) and C (0,022 wt%). A steel bar of 19,05 mm in diameter was machined into disks of 5 mm in thickness. After machining the disks were submitted to sanding with emery paper until #1000 grit size. Table 1 presents the proportions of the components in the powder mixture applied for pack aluminizing. The metal to be diffused was a fine aluminum powder, NH_4Cl was applied as the activator and Al_2O_3 as the inert compound. Samples were named after the applied pack configuration [4] and aluminizing temperature [8] (e.g. 8-2-90-4h as 8 wt% Al, 2wt% NH_4Cl and 90 wt% Al_2O_3 for 4 hours).

Table 1 – Proportion of components (wt. %) - aluminizing mixture.

Mixture	Al, %	NH_4Cl, %	Al_2O_3, %
8-2-90	8	2	90
8-5-87	8	5	87
20-2-78	20	2	78

The furnace used in the aluminizing and oxidation processes is represented in Figure 1. For the aluminization process, a vacuum pump was used to remove the air inside the furnace tube. The valve separating the pump from the rest of the system was opened and the other valves were kept closed. After that, the pump was turned off and the pump valve, closed. Argon (Ar) from a cylinder diffused through the tube driven by rarefaction and replaced the air once inside it. This last process happened by opening the valve that connects the Ar cylinder and the system. The process was repeated at least 3 times until the atmosphere inside the furnace was nearly inert. The pump valve was then closed and both valves connecting the system to the Ar cylinder and the environment were kept open to maintain a constant Ar flux of 100 ml/min. After configuring the atmosphere the furnace is ready to operate at 1173 K for pack aluminizing.

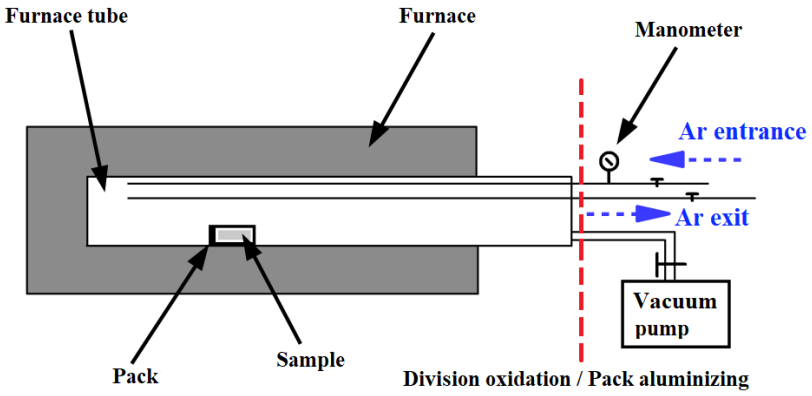

Figure 1 – Furnace scheme for the oxidation and pack aluminizing processes

Applying an analytical scale, the specimens' masses were measured before and after aluminizing and the mass gain per unit area was calculated, in order to compare the mass gain per unit area for different pack configurations.

After aluminizing, a sample of each condition was hot mounted for cross section evaluation in a FEI scanning electron microscope, model Quanta 250. Images were acquired applying a voltage of 25 kV and backscattering electrons. X-ray diffraction (XRD) analysis were performed in a D8 discover from Bruker AXS, with Mo radiation. Analyses were performed from 15º to 50º with 25 s step time and 0.02º step size.

It is important to mention that Al was chosen as the diffusion element because of the thermodynamically more stable oxide that is formed during the oxidation process, according to the *Ellingham Diagram* [9]. Besides, *Pilling-Bedworth Ratio* is closer to the unity [1].
For oxidation testing an open air furnace was used at a fixed temperature of 1173 K. The mass gain of the specimens was measured per unit area through a period of time. As the following relation is valid:

$$\frac{\Delta m}{A} \propto y$$

with *y* being the layer thickness, oxidation tests results were able to be used to build oxidation kinetic curves for each pack configuration and the substrate, in order to compare the results. SEM images and DRX data were also obtained from oxidized samples.

Logarithmic and parabolic regressions were used, following equations 1 and 2, to find the *oxidation constants* ($\varkappa$) a mathematical parameter that multiplies the oxidation kinetic equation.

$$y^2 = 2k't + const_1 \quad (1)$$

$$y = k'' \ln\left(\frac{t}{const_2} + 1\right) \quad (2)$$

This parameter ($\varkappa$) can be calculated from k’ and k’’ using the following criteria:

$$\varkappa = \sqrt{2k'} \rightarrow parabollic$$
$$\varkappa = k'' \rightarrow \log arithmic$$

This criteria is justified by the fundamental definition of $\varkappa$, which is, mathematically, the constant multiplying the kinetic equation. Constants $const_1$ and $const_2$ (on equations 1 and 2) were defined to be zero and unity, respectively, for simplicity. This constant ($\varkappa$) gives an quantitative idea of how fast an oxidation kinetics is. The smaller the $\varkappa$, the slower the kinetics and a thinner layer is formed during oxidation.

Results and discussion

Table 2 shows the mass gain per unit area of AISI 304L specimens after aluminizing. It is clear that samples submitted to a longer treatment time gain more mass due to extended Al diffusion. Activator concentration also appears to maximize Al diffusion, i.e. the more

activator the larger the mass gain per unit area. In terms of mass gain, the present experiments are consistent with the theoretical model developed by *Levine* and *Caves* [4,5]. The pack mixture with the proportion of 20-5-75 was not applied in the present research, since high Al concentrations tends to sinter the mixture therefore preventing the specimens to be removed from the pack. Additionally, high NH_4Cl concentrations showed a high probability of forming heterogeneities on specimens' surface.

Table 2 – Mass gain per unit area after pack aluminizing.

Mixture	*Δm/A (g/cm²)*	
	4 h	**8 h**
8-2-90	0,0049	0,0131
20-2-78	0,0025	0,0191
8-5-87	0,0136	0,0168

Figure 2 presents actual size photographs from the aluminized samples. As previously mentioned, higher activator concentration yields heterogeneities at the specimen surface. Such irregularities seem to be accompanied by instability on the layer, which appears to flake off when manipulated. Moreover, larger aluminium content also appears to lead to a more porous surface aspect.

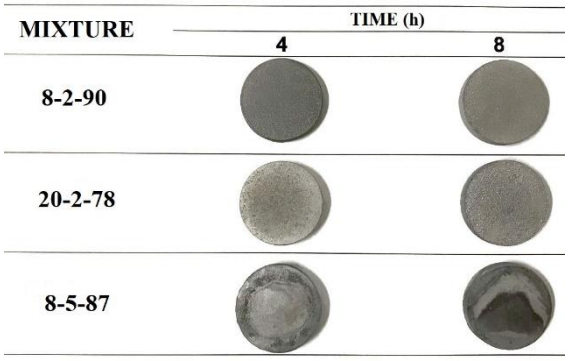

Figure 2 – Surface aspect of the samples aspects after pack aluminizing at 1173K

Microstructural characterization

Figure 3 presents backscattered scanning electron micrographs from the specimens. The micrographs clearly show the steel substrate beneath and top layers with different morphology indicating that altering pack components possibly changes the aluminide nature. The shades of grey on the images indicate regions with different composition.

By analyzing Figs. 3a-d one can also infer that, mass gain should be larger for samples exhibiting a double layer rather than a single layer. All the pack aluminizing conditions yielded a double layer except 8-2-90-4h condition, as seen in Fig. 3a.

SEM images obtained are very similar to Houngniou, Chevalier and Larpin [10], which also used NH_4Cl and Al_2O_3 as the activator and inert compound. The pack configuration used in their work was 15-3-82-5h. An intermetallic layer and a interdiffusion zone appeared between the substrate and the simple or double layer, the same as shown in Figs. 3a-d.

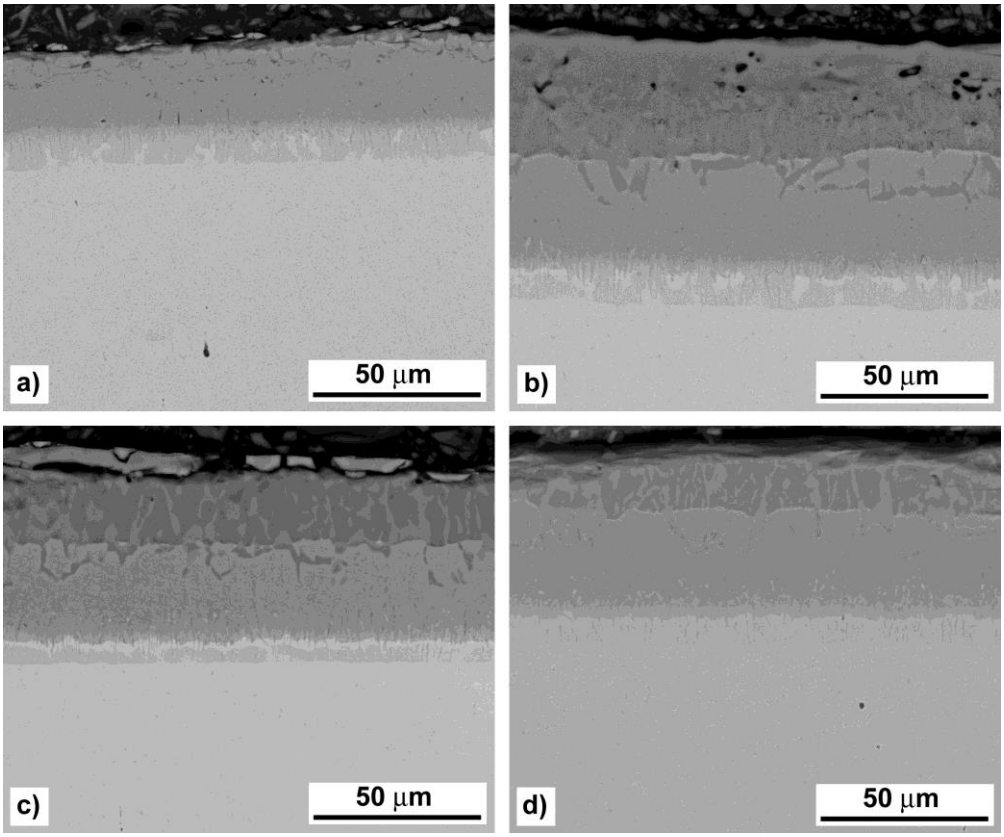

Figure 3 – SEM images of aluminized specimens (a) 8-2-90-4h (b) 8-2-90-8h (c) 8-5-87-4h (d) 20-2-78-8h.

Figure 4 presents X-ray diffraction patterns from the aluminized specimens, applying a pack mixture of 8-2-90-4h (Fig. 4a) and 8-5-87-8h (Fig. 4b). The pattern from the base steel is omitted here though it yields mainly austenite peaks, corresponding to the steel composition previously given. X-ray diffraction indicates that after aluminizing the most common aluminides produced were FeAl, Fe_2Al_5 and $FeNiAl_5$.

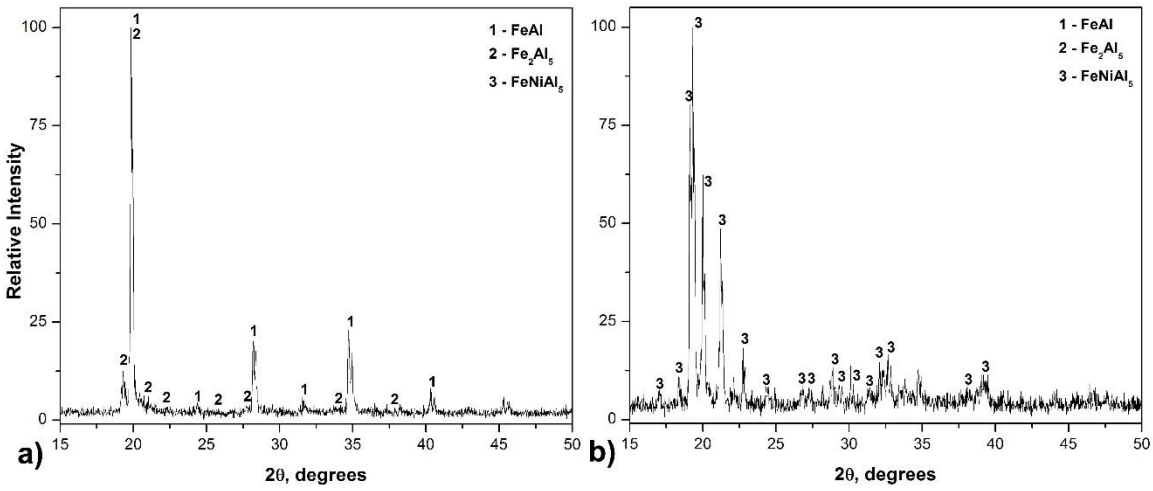

Figure 4 – X-ray diffractograms from the specimens aluminized at 1173 K with a mixture of (a) 8-2-90-4h and (b) 8-5-87-8h.

The sample aluminized for 4 h in a mixture containing 8% Al and 2% of NH_4Cl results in the presence of FeAl mostly. Additionally, weak diffraction lines corresponding to the Fe_2Al_5 are seen. Comparing such observations with the SEM images it possible to infer that Fe_2Al_5 begins to form at the top of the FeAl layer (see Fig. 3a). For longer aluminizing times (e.g. 8h), higher activator concentration or higher aluminum concentration the Fe_2Al_5 is always produced at the top of the FeAl layer. However, according to the diffractogram from Fig. 4b the element Ni substitutes an Fe leading to the $FeNiAl_5$ compound. This mixed iron-nickel aluminide is observed at the top of the micrographs shown in Figs. 3b-d.

$FeNiAl_5$ is probably formed in its hexagonal form. It was previously described by Ellner and Röhrer [11] and further obtained by Eleno, Frisk and Schneider [12]. In their paper, it is discussed that $FeNiAl_5$ lattice is still doubtful.

Figure 5 summarizes the results from the oxidation tests. Fig. 5a shows the results from specimens aluminized for 4h while Fig. 5b presents the results from the samples treated for 8h. Additionally, the oxidation curve of the AISI 304L steel substrate is shown on both figures for comparison purposes. Oxidation resistance was increased significantly for 8-2-90-4h and 8-5-87-4h samples, as shown in Fig. 5a. With the regression, it was found that 20-2-78-4h and 20-2-78-8h follows the parabolic equation, while the other samples follow logarithmic equation.

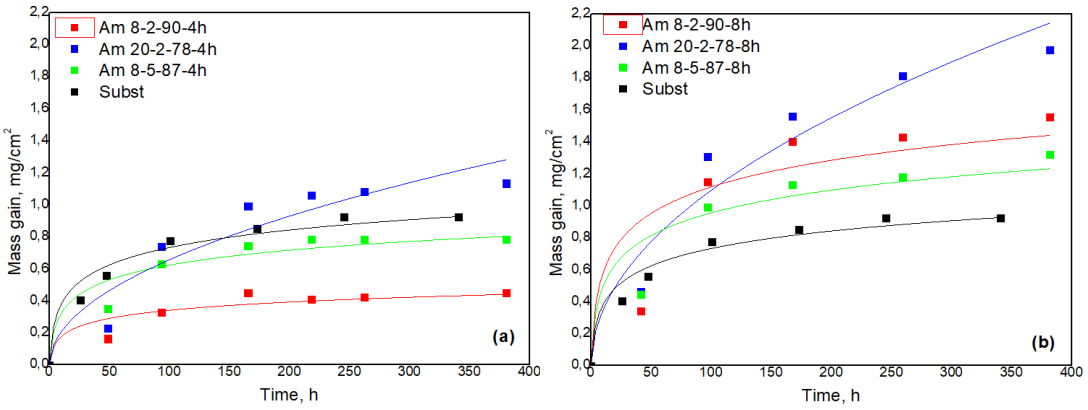

Figure 5 – Mass gain curves at 1173 K for (a) samples treated for 4h (b) samples treated for 8h.

Oxidation constants, calculated from logarithmic and parabolic regression, are exposed in Table 3.

Table 3 – Oxidation constants found with parabolic (par) and logarithmic (log) regression

Samples	**k' or k''**	$\varkappa$
Substrate (log)	0.1670 ± 0.0050	0.1670±0.0050
8-2-90-4h (log)	0.0740 ± 0.0050	0.0740±0.0050
8-2-90-8h (log)	0.2420 ± 0.0200	0.2420±0.0200
8-5-87-4h (log)	0.1350 ± 0.0060	0.1350±0.0060
8-5-87-8h (log)	0.2070 ± 0.0100	0.2070±0.0100
20-2-78-4h (par)	0.0020 ± 0.0003	0.063±0.020
20-2-78-8h (par)	0.0060 ± 0.0006	0.110±0.030

One can draw a conclusion comparing directly the values of $\varkappa$ from equations with the same mathematical nature. Considering the two equations, for a long time of oxidation exposure, a good solution to the problem is a logarithmic curve. Defining y_{log} and y_{par} the logarithmic and parabolic kinetics equation respectively, the following relation is valid:

$$\frac{d}{dt}\left(y_{\log}\right) < \frac{d}{dt}\left(y_{par}\right) \tag{3}$$

which results in slower oxidation kinetics and a thinner oxide layer for the logarithmic. It was also observed that:

$$\lim_{t \to \infty}\left(y_{\log}\right) = L \tag{4}$$

Equation 4 represents that after long time intervals, oxidation kinetics dictated by logarithmic expressions tends to have a finite asymptote L, not part of the curve's mathematical nature. This result was also observed in Tortorelli and Natesan studies [13, 14]. In the first one, FeAl oxidation kinetics on air at 973 K was evaluated. The results reinforce that oxides with logarithmic kinetics are a better solution.

It was found that, for the substrate $\varkappa = 0.1670$. Calculations showed $\varkappa_{8\text{-}2\text{-}90\text{-}4h} = 0.0740$ and $\varkappa_{8\text{-}5\text{-}87\text{-}4h} = 0.1350$. Graphical analysis reveals that both are logarithmic equations and therefore the values demonstrate a good solution to the problem.

Figure 5a shows, however, that 20-2-78-4h samples, modeled by a parabolic curve, can be a good solution for a small period of oxidation exposure, comparing with the substrate kinetics. When dealing with these situations, equalizing the logarithmic and parabolic equations gives us the points in time (t_0) which the mass gain, consequently the oxide layer thickness, is approximately the same for both kinetics. This point is a kind of frontier that indicates which pack configuration is better for a specific situation.

$$\chi_1 \ln\left(t_0 + 1\right) = \chi_2 \sqrt{t_0} \tag{5}$$

Solving Eq. 5 allows one to conclude which pack configuration is better for the specific situation. The solution to this equation is t_0. Defining t as the time of the substrate exposure to common air at 1173 K, one can infer the following set of conclusions:

$t < t_0 \rightarrow$ *parabolic kinetics pack configuration efficiency is better*

$t > t_0 \rightarrow$ *logarithmic kinetics pack configuration efficiency is better*

$t = t_0 \rightarrow$ *both have equal efficiency*

It is important to notice that this set of conclusions are only valid if $\varkappa_1 > \varkappa_2$, since if the opposite happens the only solution to equation 5 is $t = 0$, which physically does not add any new information to the problem. This solution is explained by mathematical nature of the curves showed in Eq. 3.

The same kind of evaluation is valid if dealing with two pack configurations that obeys the rules: I) Both have $\varkappa$ numerically lower than the substrate's $\varkappa$; II) one of them obeys a logarithmic kinetics with oxidation constant $\varkappa_1$ and the other obeys a parabolic kinetics with oxidation constant $\varkappa_2$; III) $\varkappa_1 > \varkappa_2$. In this situation, one can, from Eq. 5 and the set of conclusions driven by its solution, decide which pack configuration is better for the

problem. This scenario can be seen comparing 8-5-87-4h and 20-2-78-8h samples' oxidation kinetics.

Figure 6 shows backscattered SEM micrographs from the oxidized AISI 304L steel specimen (Fig. 6a) and an oxidized sample which was previously aluminized applying a mixture of 8-2-90-8h (Fig. 6b).

The steel substrate yields a thin homogeneous oxide layer with few perpendicular cracks. Additionally, it is possible to note that oxidation proceeds beneath this layer through the grain boundaries. As previously analyzed, at 1173 K, this is a relatively fast growing oxide. Below this corroded region the substrate appears as a single phase, most likely consisting of austenite.

Fig. 6b presents a sample which was previously aluminized with a pack mixture of 8-2-90-8h, before oxidation (Fig. 3b shows the as aluminized layer). It is possible to note that Al rich phases redistributes during the oxidation test. The double layer previously seen is replaced by a very deep Al diffusion zone. This region is composed of two phases and additional porosity on the surface and midway towards the substrate. Also some aluminide layers revealed orthogonal cracks after oxidation.

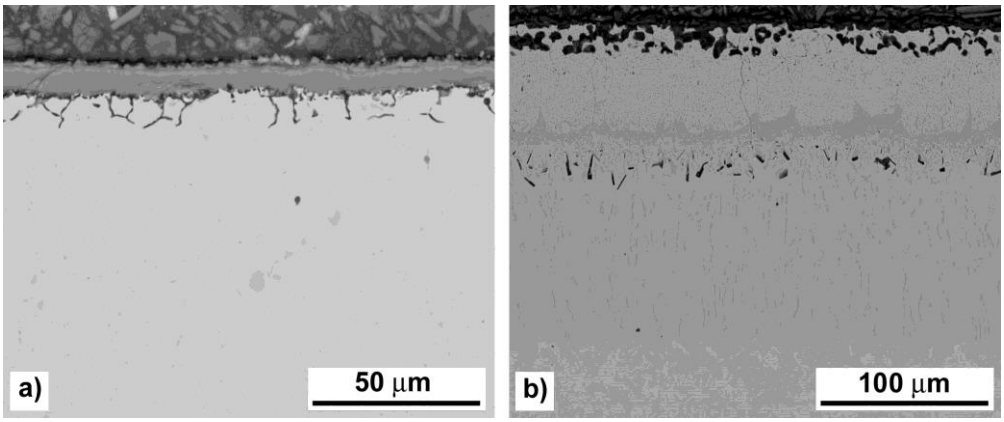

Figure 6 – Oxidized samples (a) non-aluminized substrate and (b) 8-2-90-8h aluminized.

Samples treated with a mixture of 8-2-90-4h and 20-2-78-4h did not present any orthogonal cracks, which is a different scenario comparing to the double layers produced after 8h of aluminizing which developed orthogonal cracks during oxidation. Once generated, cracks increase the surface area, which tends to lead towards larger mass gain during oxidation. Relating this result with its $\varkappa$ value, one can infer that orthogonal cracks are fundamentally related with higher $\varkappa$ values. Voids can also be observed on the oxidized samples, due to the *Kirkendall Effect* [15].

X-ray diffraction was additionally performed on the surface of the oxidized specimens. The results are shown in Figure 7. For the untreated AISI 304L steel (Fig. 7a) mainly a mixed oxide of the Fe_2O_3 type is noticed. It is expected that Cr also appears in the oxide as a substitute to Fe. Additionally, some diffraction lines from the austenitic substrate are seen.

All the oxidized specimens, after aluminizing, yielded a very similar diffractogram showing the FeAl iron aluminide plus Al_2O_3 in small quantities. In some cases the peak positions from the FeAl aluminide are slightly shifted which is explained based on the variable Fe/Al ratio on this cubic aluminide. Fig. 7b shows an example of a diffractogram from an oxidized specimen which was previously aluminized with a mixture of 8-5-87-8h.

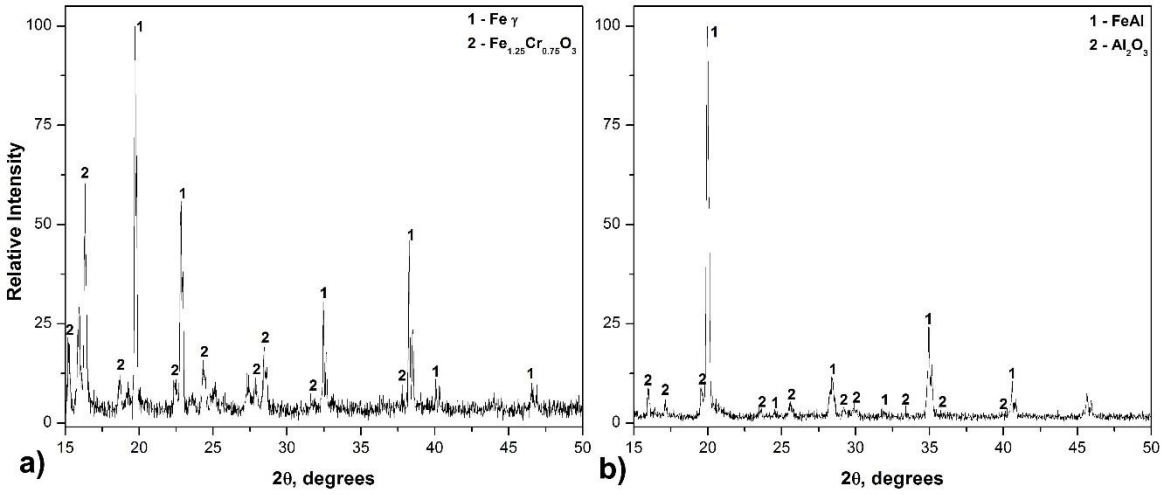

Figure 7 – XRD data from the oxidized (a) non-aluminized substrate and (b) 8-5-87-8h.

The appearance of alpha alumina (α-Al_2O_3) in the aluminized samples, in comparison to the non-aluminized substrate (Fig. 7a), is well explained thermodynamically by the *Ellingham diagrams* [9], since it is a more stable oxide. It was also described by Grabke that upon FeAl oxidation, γ-, δ- and θ-Al_2O_3 are previously formed and it slowly transforms into the more stable α-Al_2O_3 [16]. Thus, one can infer that the transformation process was achieved and α-Al_2O_3 is already the main oxide.

Conclusions

Varying the activator proportion and aluminum powder content, on a pack aluminizing process, implies on a thicker, thinner, simple or double layer. It does not mean, however, that it is a more protective coating, with respect to the high temperature corrosion protection. Using logarithmic and parabolic regression, an oxidation constant may be defined to compare different oxidation kinetics. XRD analysis showed the formation of FeAl and $FeNiAl_5$, after pack aluminizing of the AISI 304L steel. SEM images indicate that samples with a single layer the intermetallic produced was the FeAl and, if pack aluminizing continues, a $FeNiAl_5$ top layer is formed, therefore creating a double layer. XRD data also shows an important formation of α-Al_2O_3 during the high temperature oxidation testing, which is in agreement with previous works. FeAl layers appear to have a better efficiency when facing high temperature oxidation, as shown by its kinetics. Furthermore, experiments indicate that on thicker layers, orthogonal cracks tend to appear, allowing oxygen to penetrate the redistributed intermetallic coating. *Kirkendall effect* voids were additionally observed in oxidized samples cross sections.

Acknowledgments

The authors acknowledge the Multi-User Central Facilities (CEM/UFABC) for the experimental support, ALCOA for supplying the aluminum and alumina powders and the scholarship granted to D.D.M.R. Ferreira.

References

1. R. Winston Revie, H. H. Uhlig, **Corrosion and corrosion control** - An introduction to Corrosion Science and Engineering, 4. ed., USA: Wiley, 2008, pg.1-5.
2. J. Stringer, High-temperature corrosion of superalloys, **Materials Science and Technology**, 3:7, Palo Alto, Cal., USA, 1987, 482 – 493.
3. M. C. L. Patterson , S. He , L. L. Fehrenbacher , J. Hanigofsky & B. D. Reed (1996) Advanced HfC-TaC Oxidation Resistant Composite Rocket Thruster, **Materials and Manufacturing Processes**, 11:3, 2007, 367-379.
4. N. Kandasamy, L.L. Seigle, F.J. Pennisi, The kinetics of gas transport in Halide-Activated Aluminizing Packs, **Metallurgical and Protective Coatings**, USA, 1981, pg. 17-27.
5. S.R. Levine, R.M. Caves, Thermodynamics and Kinetics of Pack Alluminide Coating Formation on IN-100, **Journal of the electrochemical society**, USA, 1974, pg. 1051-1065.
6. H. H. Uhlig, Initial oxidation rate of metals and the logarithmic equation, **Acta Metallurgica**, USA, Vol. 4, 1956, pg. 541-554.
7. C. Wagner, Atom movement, **American Society for Metals**, Cleveland, OH, 1951, pg. 153-173.
8. G.H. Meier, C. Cheng, R.A. Perkins, W. Bakker, Diffusion chromizing of ferrous alloys, **Surface and Coatings Technology**, vol. 39-40, part 1, USA, v. 39-40, p. 53-64, 1989.
9. C. Borgnakke, R. E. Sonntag, **Fundamentos da termodinâmica**, 2. Ed., São Paulo, coordenação e tradução de Roberto de Aguiar Peixoto, Blucher, 2018.
10. C. Houngniou, S. Chevalier, J. P. Larpin, High-Temperature-Oxidation Behavior of Iron-Aluminide Diffusion Coatings, **Oxidation of Metals**, Vol. 65, Dijon, France, pg. 409-439, 2006.
11. M. Ellner, T. Röhrer, Zur Struktur der ternären Phase FeNiAl5, **Materials research and advanced techniques**, Vol 81, Max Planck institute Metallforschung, Germany, 1990, pg. 847-849.
12. L. Eleno, K. Frisk, A. Schneider, Assessment of the Fe-Ni-Al system, **Intermetallics** 14, Max Planck institute for iron research, Department of materials technology, Germany, 2005, pg. 1276-1290.
13. P.F. Tortorelli, K. Natesan, Critical factors affecting the high-temperature corrosion performance of iron aluminides, **Materials Science & Engineering A258**, USA, 1998 pg. 115-125.
14. K. Natesan, Corrosion performance of iron aluminides in mixed-oxidant environments, **Materials Science & Engineering A258**, USA, 1998, pg. 126-134.
15. F. Seitz, On the theory of the Kirkendall Effect, **Journal of the physical society of Japan**, Vol. 10, No. 8, USA, 1955, pg. 679-685.
16. H. J. Grabke, Oxidation of NiAl and FeAl, **Intermetallics 7**, Max Planck Institute for iron research, Germany, 1999, pg 1153-1158.